Received: 26 November 2023 | Revised: 11 April 2024 | Accepted: 11 April 2024

DOI: 10.1111/epi.17996

Epilepsia®

RESEARCH ARTICLE

Neuronal synchrony and critical bistability: Mechanistic biomarkers for localizing the epileptogenic network

Sheng H. Wang[1,2,3,4] | **Gabriele Arnulfo**[5] | **Lino Nobili**[6,7] | **Vladislav Myrov**[2] | **Paul Ferrari**[8,9] | **Philippe Ciuciu**[3,4] | **Satu Palva**[1,10,11] | **J. Matias Palva**[1,2,10]

[1]Neuroscience Center, Helsinki Institute of Life Science, University of Helsinki, Helsinki, Finland

[2]Department of Neuroscience and Biomedical Engineering, Aalto University, Espoo, Finland

[3]Le Commissariat à l'énergie atomique et aux énergies alternatives, NeuroSpin, Université Paris-Saclay, Gif-sur-Yvette, France

[4]Models and Inference for Neuroimaging Data, Inria, Palaiseau, France

[5]Department of Informatics, Bioengineering, Robotics, and System Engineering, University of Genoa, Genoa, Italy

[6]Child Neuropsychiatry Unit, Istituto di Ricovero e Cura a Carattere Scientifico Istituto Giannina Gaslini, Member of the European Reference Network EpiCARE, Genoa, Italy

[7]Department of Neurosciences, Rehabilitation, Ophthalmology, Genetics, and Maternal and Children's Sciences, University of Genoa, Genoa, Italy

[8]Jack H. Miller Magnetoencephalography Center, Helen DeVos Childrens Hospital, Grand Rapids, Michigan, USA

[9]Department of Pediatrics and Human Development, Michigan State University, East Lansing, Michigan, USA

[10]Centre for Cognitive Neuroimaging, School of Psychology and Neuroscience, University of Glasgow, Glasgow, UK

[11]Division of Psychology, Values, Ideologies and Social Contexts of Education, Faculty of Education and Psychology, University of Oulu, Oulu, Finland

Correspondence
Sheng H. Wang, Neuroscience Center, Helsinki Institute of Life Science (HiLIFE), University of Helsinki, Helsinki, Finland.
Email: sheng.wang@helsinki.fi

Funding information
The Academy of Finland, Grant/Award Number: SA 253130 and SA 296304; Sigrid Jusélius Foundation; Finnish Cultural Foundation, Grant/Award Number: 00220071; French National Research Agency (ANR) DARLING project, Grant/Award Number: Projet-ANR-19-CE48-0002; Ella and Georg Ehrnrooth Foundation, Grant/Award Number: 14-10553-2; NEXTGENERATIONEU (NGEU), Grant/Award Number: MNESYS (PE0000006); The Sigrid Jusélius Foundation, Grant/Award Number: 210527

Abstract

Objective: Postsurgical seizure freedom in drug-resistant epilepsy (DRE) patients varies from 30% to 80%, implying that in many cases the current approaches fail to fully map the epileptogenic zone (EZ). We aimed to advance a novel approach to better characterize epileptogenicity and investigate whether the EZ encompasses a broader epileptogenic network (EpiNet) beyond the seizure zone (SZ) that exhibits seizure activity.

Methods: We first used computational modeling to test putative complex systems-driven and systems neuroscience-driven mechanistic biomarkers for epileptogenicity. We then used these biomarkers to extract features from resting-state stereoelectroencephalograms recorded from DRE patients and trained supervised classifiers to localize the SZ against gold standard clinical localization. To further explore the prevalence of pathological features in an extended brain network outside of the clinically identified SZ, we also used unsupervised classification.

Results: Supervised SZ classification trained on individual features achieved accuracies of .6–.7 area under the receiver operating characteristic curve (AUC). Combining all criticality and synchrony features further improved the AUC

to .85. Unsupervised classification discovered an EpiNet-like cluster of brain regions, in which 51% of brain regions were outside of the SZ. Brain regions in the EpiNet-like cluster engaged in interareal hypersynchrony and locally exhibited high-amplitude bistability and excessive inhibition, which was strikingly similar to the high seizure risk regime revealed by our computational modeling.

Significance: The finding that combining biomarkers improves SZ localization accuracy indicates that the novel mechanistic biomarkers for epileptogenicity employed here yield synergistic information. On the other hand, the discovery of SZ-like brain dynamics outside of the clinically defined SZ provides empirical evidence of an extended pathophysiological EpiNet.

KEYWORDS

bistability, classification, criticality, epileptogenic zone, synchrony

1 | INTRODUCTION

Epilepsy is characterized by an enduring predisposition to having seizures.[1,2] An epileptic seizure can be referred to various abnormal neuronal activities or hypersynchrony.[3,4] Thirty percent to 40% of epilepsy patients have drug-resistant epilepsy (DRE), where antiseizure medications fail to control the seizures. The last resort treatment for DRE is surgery that aims to resect the brain tissue responsible for seizure generation, commonly known as the epileptogenic zone (EZ). Nonetheless, large variability in postsurgical seizure freedom (30%–80%)[5,6] implies that current biomarkers fail to fully localize the EZ in many patients.[7–9] New approaches to deepen the understanding of the systems-level mechanisms of epileptogenicity and their individual expression are thus urgently needed.

In patients with focal seizure onset, seizure activity is often limited to a small number of brain areas.[10] Clinically identifying the EZ involves visual inspection of stereoelectroencephalographic (SEEG) traces during seizure onset and propagation, while considering semiology and other mechanistic characteristics, such as lesions,[11] metabolic[12] or neurophysiological anomalies including high-frequency oscillations,[9] spikes,[13] and concurrent slow and fast abnormal activity.[14] In light of evidence suggesting that the existence of a broader connected epileptiform network portends poor surgical outcomes, it has been increasingly recognized that epilepsy is a brain network disease rather than attributable to isolated lesions.[15–19]

Synchrony in brain networks is thought to be instrumental for neuronal communication.[20] Previous SEEG studies have shown that during interictal periods, pathological regions are more synchronized.[21] Synchrony levels in the brain are predicted by individual positions in a criticality state-space so that synchrony is moderate in healthy brains but more elevated in epileptic brains.[22] This evidence supports the hypothesis of criticality being a hallmark of healthy brain function and shifting toward supercriticality being characteristic of epileptogenicity.

Key points

- We advanced novel complex systems-driven and systems neuroscience-driven biomarkers for epileptogenicity.
- Increased bistability, inhibition, and scaling exponents characterized both the model operating in a high seizure-risk regime and the SEEG oscillations recorded from the seizure zone.
- Combining all biomarkers yielded more accurate supervised SZ classification than using any individual biomarker alone.
- Unsupervised classification revealed more extended pathological brain networks including the SZ and many non-SZ areas that were previously considered healthy.

The *brain criticality* hypothesis posits that healthy brains operate near a phase transition (PT) between asynchrony and synchrony.[22,23] Its hallmarks include moderate levels of synchrony with a unimodal distribution (Figure 1C, bottom), emergent long-range temporal correlations (LRTCs),[24] and balanced excitation/inhibition (E/I).[25,26] Shifting toward either lower (subcriticality) or higher (supercriticality) levels of synchrony than what is required for characterizing criticality has been associated with brain disorders.[27] In particular,

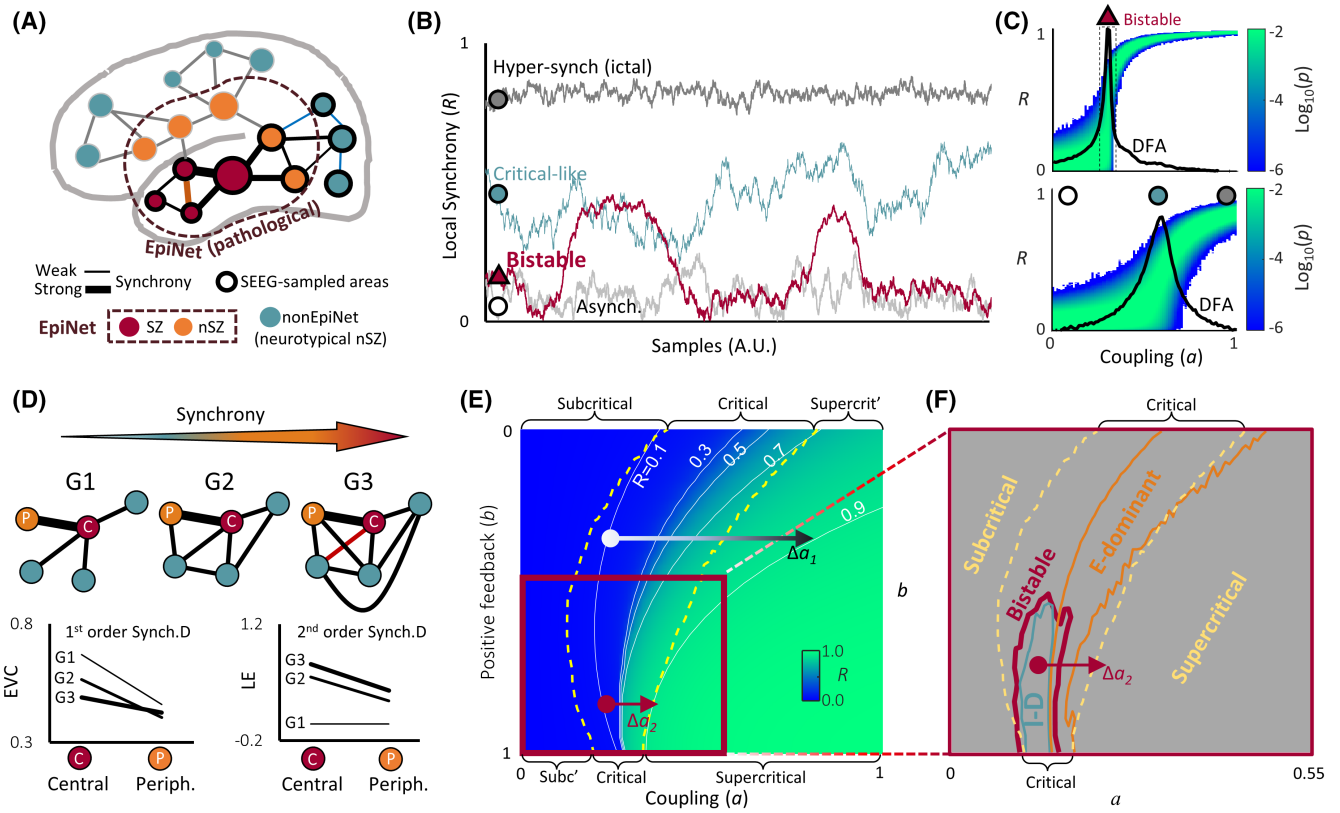

FIGURE 1 Hypothesis: aberrant local criticality and strong interareal synchrony concurrently characterize spontaneous activity of the epileptogenic network (EpiNet). (A) Seizure zone (SZ) shows seizure activity. The pathological EpiNet might comprise the SZ and some non-SZ (nSZ), and the latter was previously considered healthy. Stereoelectroencephalographic (SEEG) electrode insertion is driven by clinical hypothesis and thus might miss some pathological areas. (B) Synchrony (R) when the model is in different regimes. R is the amplitude envelope of the complex-valued mean field. (C) The probability distribution (p) of R samples and mean DFA exponents of R (black line) as the model was controlled by strong (top) and weak (bottom) local positive feedback; the corresponding time series were shown in panel B. DFA, critical exponent obtained using detrend fluctuation analysis. (D) As synchrony increased, first- and second-order synchrony derivatives of central nodes were consistently larger than that of peripheral nodes. EVC, eigen vector centrality; LE, local efficiency. (E) Time-averaged R of the model. The area encompassed between two dashed lines represents the critical regime wherein DFA > .6; Δa_1 and Δa_2 indicate the coupling increment required to drive the model from critical oscillations ($R = .1$) to supercritical hypersynchrony ($R = .9$) in classical critical and bistable critical regimes, respectively. (F) Association between criticality, bistability, inhibition dominance (I-D), and excitation (E) dominance. The y-axis in panels E and F was reversed to make them comparable with the cusp fold (Figure S1).

neuronal activity in epileptic brains exhibits signs of supercriticallike dynamics.[22,28] The classic brain criticality postulates the PT to be continuous (second order).[23] However, canonical firing rate models,[29] ensemble dynamics models,[30] and models for synchronization dynamics[31] have also predicted a discontinuous (first order) PT (Figure 1B). Empirically, operation at a discontinuous PT would lead to bistability such as the switching between up and down states during sleep in animal electrophysiological data[32,33] and periods of high and low synchrony in human resting-state electroencephalography,[34] magnetoencephalography, and SEEG.[31] Theoretical work has suggested bistability to occur near criticality when ensembles are influenced by positive feedback[31,35] or constrained by activity-limiting mechanisms due to overexcitation.[36]

Elevated bistability has been suggested as a universal indicator of a predisposition to catastrophic events characterized as sudden, uncontrollable bursts of hypersynchrony seen in various complex systems.[37,38] We posit that epileptic seizures could be construed as this kind of catastrophic runaway neuronal synchrony. This notion implies that bistability in spontaneous neuronal activity could be a mechanistic biomarker for seizure risk.[31]

We hypothesized that an epileptogenic network (EpiNet) could comprise multiple components, some of which may overlap (Figure 1A).[39] Not all of the components are involved in every observed seizure or display pathological features that are commonly recognized. Regions inside EpiNet would spontaneously operate in a high bistability critical regime that primes them to catastrophic seizure events. This aberrant local criticality

should coexist with a large-scale trend toward supercriticality, characterized by elevated synchrony around the EpiNet.[22] As synchrony increases (G1–G3 in Figure 1D), central nodes in the EpiNet exhibit stronger connectivity compared to peripheral nodes. Meanwhile, connectivity within the neighborhood of the EpiNet also increases. These two phenomena can be assessed using first- and second-order connectivity metrics, respectively.

To test this hypothesis, we assessed the potential of combining bistability, classic criticality, and synchrony assessment as holistic, mechanistic biomarkers for epileptogenicity in models and in interictal awake resting-state SEEG. The resting-SEEG features may be used to train supervised classifiers to identify seizure zone (SZ) against gold standard clinical localization. To investigate whether the pathological networks extend beyond the SZ (i.e., the EpiNet), unsupervised classification may be employed to test whether certain regions inside the non-SZ (nSZ) exhibit pathological features similar to the SZ.

2 | MATERIALS AND METHODS

2.1 | Subjects and recording

We studied 64 patients (mean ± SD age = 29.7 ± 9.5 years, 29 females) with focal onset seizures treated at the Niguarda "Ca′ Granda" Hospital, Milan, Italy. They underwent SEEG for the first time and had no prior brain surgeries. Ten minutes of resting-state SEEG was obtained as monopolar local field potentials. There were no seizures at least 1 h before and after the recordings. All patients were under antiseizure medication with variable active compounds and dosages (Table S1). The recording time from the last drug administration was not controlled, and the drug effects were not considered.

To ensure enough samples for within-subject SZ classification, we required each subject to have at least five SZ and five nSZ contacts. This led to the selection of 55 subjects for the analysis, who on average had 28.5 ± 17.0 SZ and 66.4 ± 21.2 nSZ contacts.

2.2 | Clinical identification of SZ

Physicians identified the SZ by visual analysis of the SEEG traces. Various peri-ictal and ictal events may initiate from the seizure onset zone (SOZ), including low-voltage fast discharge, spike-and-wave, and polyspike slow bursts.[4] Brain areas inside the seizure propagation zone (SPZ) do not initiate seizures and often show delayed, rhythmic modulation after seizure initiation from the SOZ.[15,17] It is also common for physicians to identify contacts as both SOZ and SPZ simultaneously, referred to as SOPZ. In this study, we referred to SOZ, SPZ, and SOPZ collectively as the SZ. All samples not identified as SZ were classified as tentatively healthy nSZ.

2.3 | Assessing criticality

Narrowband frequency amplitudes were obtained by convoluting the broadband data with Morlet wavelets ($m = 5$) from 2 to 225 Hz with equal interfrequency distance on $\log_{10}$ scale. We subsequently assessed LRTCs, bistability, and E/I balance for narrowband oscillations (formal definitions in Supplementary Materials).

The critical exponent, obtained using detrend fluctuation analysis (DFA), was used to assess LRTCs.[24] The DFA exponent is capable of predicting fluctuations in a one-dimensional time series over a long temporal range using a small fraction of the data; $.5 < \text{DFA} < 1$ indicates significant LRTCs (i.e., an indication of criticality), $\text{DFA} = .5$ indicates random-walk, and $1 < \text{DFA} < 2$ suggests nonstationarity or unbounded growth.

The BiS index quantifies the degree of bistability of an oscillation.[34] Empirically observed probability distribution of a narrowband power is fitted with a single exponential and a biexponential model. The BiS is a scalar derived from the model comparison between the two competing models based on Bayesian information criterion. BiS >3 indicates bistability.

The fE/I index makes inferences about the operational regime of an oscillation based on the relationship between time-resolved DFA and local synchrony.[26] fE/I = 1 with a constraint of $.5 < \text{DFA} < 1$ indicates balanced E/I; $0 < \text{fE/I} < 1$ indicates I-dominance, and $1 < \text{fE/I} < 2$ indicates E-dominance.

2.4 | Assessing synchrony derivatives

Interareal synchrony was assessed using the phase-locking value (PLV) for 50 narrowband frequencies (Morlet wavelets, $m = 7.5$) spanning from 2 to 450 (Supplementary Materials). We treat each PLV matrix as a graph, wherein contacts are nodes and synchronizations are edges. We estimated first-order synchrony derivatives using effective weight (We) and eigenvector centrality (EVC). We is the weighted sum of edges connected to a node. EVC is a self-referential centrality, so that a node has high EVC if its neighbors have high EVC. We assessed second-order synchrony derivatives using clustering coefficient (Cc) and local

efficiency (LE). Cc is the fraction of node's neighbors that are also neighbors of each other. LE is the efficiency assessed in the neighborhood of a given node, where efficiency is the average inverse shortest pathlength.

3 | RESULTS

3.1 | Positive feedback in a computational model leads to bistability and increased risk for seizurelike hypersynchrony

To investigate the emergence of seizurelike hypersynchrony in systems with separately controllable bistability and criticality, we used a Kuramoto model[22] equipped with feedback.[31] The Kuramoto model generates time series characterized by emergent synchrony. Synchrony is quantified by order (R) so that $R=0$ is the absence of synchrony and $R=1$ indicates perfect synchrony (Supplementary Materials). In our model, the order is influenced by coupling strength and the weight of positive feedback. Bistability in order only emerges with an increase in positive feedback. This was expected, as positive feedback is a generative mechanism for bistability in both canonical[30,37] and generative[35,36] models.

We assessed LRTCs in the model order using the DFA exponent (see Section 2.3). Across all levels of feedback, increasing coupling led to the emergence of LRTCs at moderate levels of order, suggesting a critical regime (demarcated by the enclave within two yellow dashed lines wherein DFA > .6, Figure 1E). Only in the presence of strong feedback, the model exhibited bistable dynamics within the critical regime (Figure 1F; more details in Figure S2).

Inside the bistable regime, the model became hypersensitive to changes in coupling and could erratically transit from criticality to supercriticality. For example, a 15% increase in coupling could drive the model from the subcritical side within the critical regime with low synchrony ($R=.1$) into a supercritical regime with seizurelike hypersynchrony ($R=.9$); in contrast, at low levels of feedback, a 61% increase in coupling was needed to drive the model to exhibit the same critical-to-supercritical transition (see Δa_1 vs Δa_2 in Figure 1E).

Lastly, within the bistable regime, the excitation (E)-dominant regime is closer to supercriticality than the inhibition (I)-dominant regime (Figure 1F). In the I-dominant regime, LRTCs increase with increasing order, whereas in the E-dominant regime, LRTCs decrease with increasing order. This indicates approaching and departing from the global maximum of LRTCs, respectively (trajectory along [3, 4, 5] in Figure S2I,J).

3.2 | SZ exhibits aberrant criticality and elevated synchrony

We assessed local criticality and interareal synchrony in interictal, awake resting-state SEEG local field potentials. We then examined whether these measures can be used to differentiate SZ from nSZ.

Amplitude envelope of neuronal oscillations reflects local synchrony and is equivalent to the model order, and criticality of narrowband SEEG was assessed in the same manner as for the model. We estimated interareal synchrony between SEEG contacts with the PLV, which was then used to obtain the first- and second-order synchrony derivatives (i.e., a contact's own and its neighbors' connectivity), respectively (Figure 1D).

Visual inspection of individual data revealed differences between SZ and nSZ contacts. The SZ contacts typically exhibited stronger bistability in broadband and narrowband traces than adjacent nSZ contacts (Figure 2A,B, Figure S3). In a representative subject, the SZ was characterized by more pronounced bistability, stronger LRTCs, and I-dominance in the 80-Hz PLV graph than the nSZ (Figure 2C,D). Meanwhile, the SZ contacts and their neighbors exhibited more pronounced connectivity in the 4-Hz PLV graph (Figure 2E,F). In this subject, the SZ exhibited larger BiS and DFA estimates from 20 to 300 Hz (Figure 2G) and increased We, EVC, and Cc from 2 to 80 Hz (Figure 2H).

On the cohort level, oscillation amplitudes followed a power law distribution in frequencies of >10 Hz (Figure 3A). The SZ exhibited increased bistability and I-dominance in 45–225-Hz and 15–30-Hz ranges (Figure 3B,C) and slightly stronger LRTCs at 2–5 Hz and >100 Hz (Figure 3D). The SZ showed elevated first- and second-order connectivity (Figure 3E,F, respectively).

3.3 | Preparing band-collapsed features for SZ classification

We chose 55 subjects for the SZ classification analysis, ensuring that each had a minimum of five SZ and five nSZ contacts (Materials and Methods). Each contact was characterized by 260 features, challenging both efficient training of the classifiers and straightforward result interpretation. Spatial similarity analyses revealed distinct frequency clusters for criticality and synchrony feature maps, and we chose to use separate frequency bands for collapsing (See Supplementary Materials 1.5 and Arnulfo et al.[40] for details). Subsequently, 20 narrowband criticality features were collapsed into four bands and 50 synchrony features into six bands (defined on top of Figure 3B–D and Figure 3E,F, respectively).

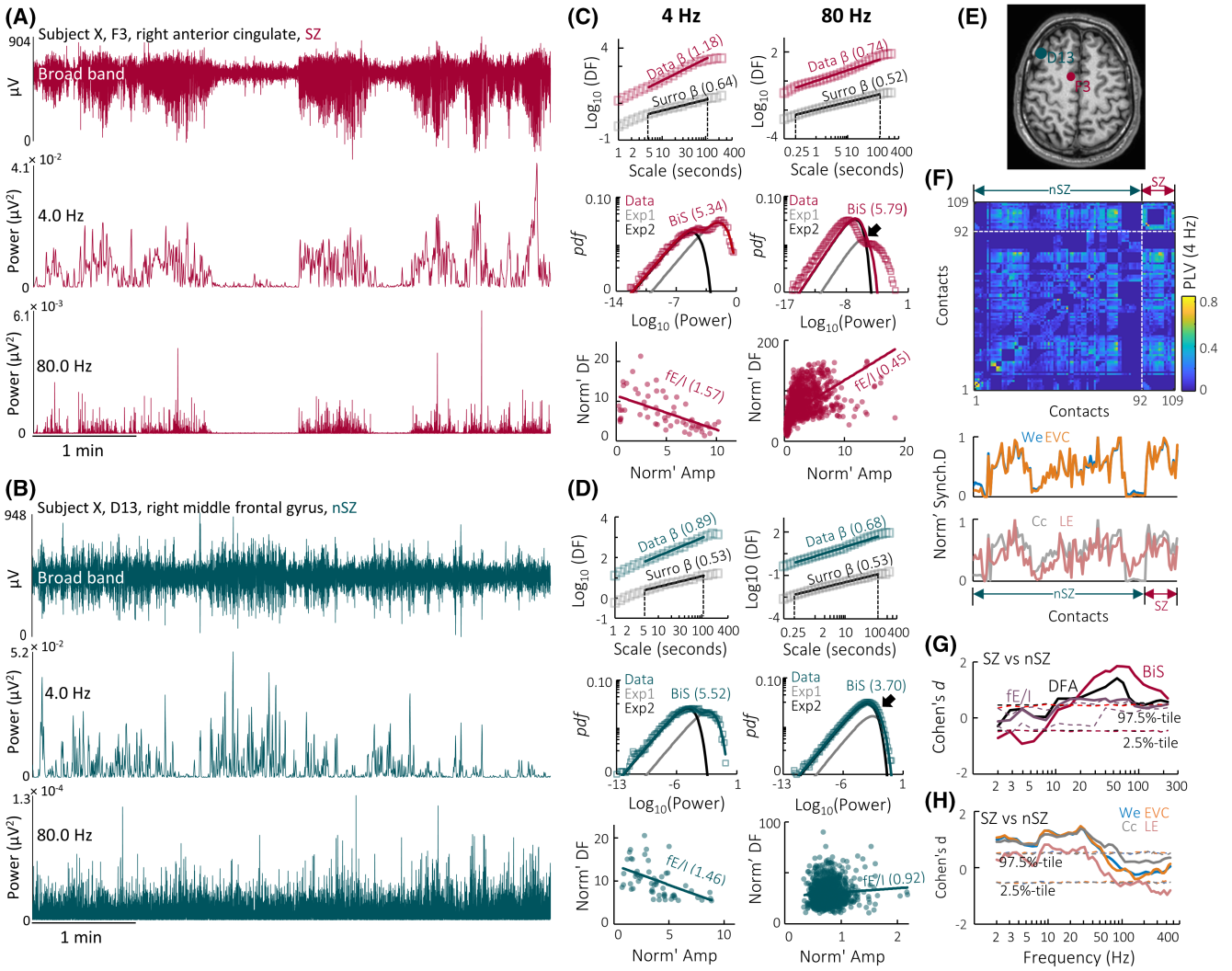

FIGURE 2 Individual level evidence of differences between seizure zone (SZ) and non-SZ (nSZ). (A and B) Five minutes of broadband and narrowband traces from (A) an SZ contact and (B) an nSZ contact from the frontal region of a representative subject. (C) The fitting of the detrend fluctuation analysis (DFA) exponent (top), BiS index (middle), and fE/I index (bottom) for 4- and 80-Hz oscillation from panel A. Markers and solid lines indicate observed data and fitted models, respectively. Amp, amplitude envelope; DF, detrend fluctuation; Norm', normalized; pdf, probability distribution function. (D) The same as panel C for panel B. (E) Stereoelectroencephalographic (SEEG) contact locations for panels A and B. (F) Top: Subject X's 4-Hz phase synchrony between all contacts assessed using phase-locking value (PLV). Bottom: Normalized synchrony derivatives of the SEEG contacts from the 4-Hz PLV matrix. Cc, clustering coefficient; EVC, eigen vector centrality; LE, local efficiency; Norm' Synch.D, normalized synchrony derivatives; We, effective weight. (G and H) Difference between SZ and nSZ in (G) narrowband criticality assessments and (H) synchrony derivatives. Dashed lines indicate confidence intervals observed from 1000 label-shuffled surrogate (Surro) data.

As a result, each contact was characterized by 36 band-collapsed features.

Compared to nSZ contacts, the SZ contacts exhibited stronger bistability and I-dominance in $\gamma_{1,2}$ (45–225) and β (15–30 Hz) band as well as larger δ (2–4 Hz) band LRTCs (Figure 3G), a form of aberrant criticality highly similar to the model dynamics in the high seizure risk regime. The SZ contacts showed elevated first- and second-order connectivity in the δ–θ (2–5.4 Hz) followed by the γ_1 (40–96 Hz) band (Figure 3H). This indicated that the SZ contacts were central nodes (Figure 1D) characterized by elevated resting connectivity to SZ and between the neighbors of SZ.

3.4 | Supervised classifier: Combining criticality and synchrony assessments maximizes SZ classification accuracy

We investigated whether criticality and synchrony assessments could be utilized to classify physician-diagnosed SZ, a fundamental prerequisite for clinical applicability. We

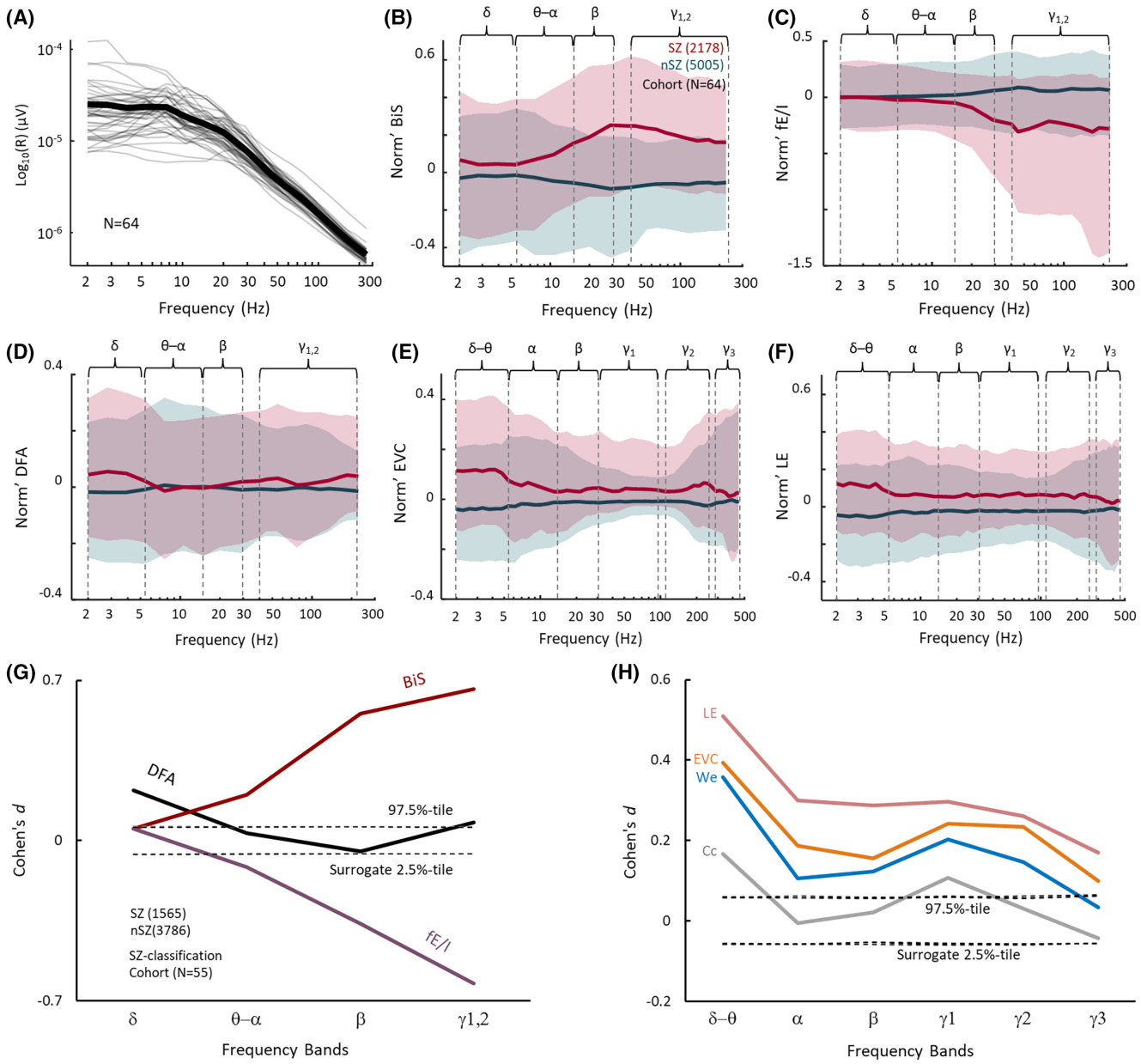

FIGURE 3 Criticality and synchrony assessments differentiated seizure zone (SZ) and non-SZ (nSZ) on the population level. (A–F) Demographics of the whole cohort samples ($N = 64$). (A) Within-subject (thin) average and group average (thick) stereoelectroencephalographic (SEEG)amplitudes. (B–F) Normalized narrowband frequency criticality and synchrony assessments for SZ and nSZ contacts. Shades indicate 25% and 75% percentiles; frequency clusters of criticality: δ (2–4 Hz), θ–α (5.4–11 Hz), β (15–30 Hz), and $\gamma_{1,2}$ (45–225 Hz); frequency clusters of synchrony: δ–θ (2–5.4 Hz), α (6.1–13 Hz), β (15–30 Hz), γ_1 (40–96 Hz), γ_2 (110–250 Hz), and γ_3 (270–450 Hz). (G and H) Differences between SZ and nSZ in band-collapsed criticality (G) and synchrony (H) assessment for the subcohort ($n = 55$) used in the SZ classification. Dashed lines indicate confidence interval observed from 10^4 label-shuffled surrogates conducted independently for each metric. Cc, clustering coefficient; DFA, detrend fluctuation analysis; EVC, eigen vector centrality; LE, local efficiency; Norm', normalized; We, effective weight.

trained supervised classifiers for SZ in three steps: (1) we assessed the similarity between criticality and synchrony assessments; (2) as a proof-of-concept, we conducted a cohort level cross-validation; and (3) We conducted within-patient SZ classification.

First, feature similarity was assessed as Spearman correlations coefficients between band-collapsed features (Supplementary Methods). The BiS and DFA assessments were positively correlated between bands (red box in Figure 4A) and negatively correlated with fE/I (blue box in Figure 4A). This constituted the first empirical evidence of concurring bistability and I-dominance in SZ, supporting the model prediction in a high-risk regime, but not in a high-bistability and E-dominant regime immediately

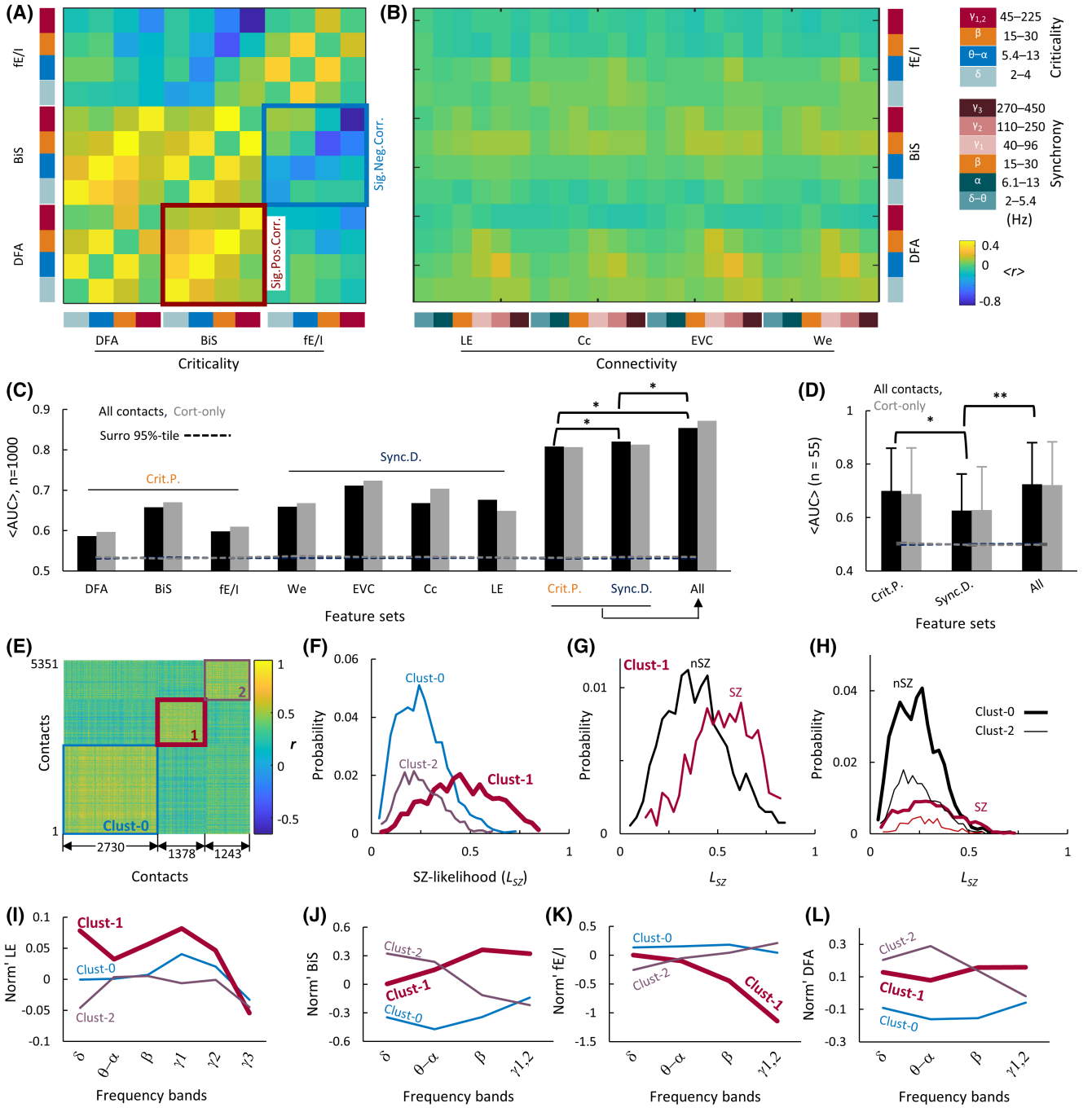

FIGURE 4 Achieving optimal seizure zone (SZ) classification by combining all criticality and synchrony features. (A) Mean within-patient Spearman correlation (<*r*>) between band-collapsed criticality assessments. (B) Similarity between criticality and connectivity across frequencies. (C) Population pooled stereoelectroencephalographic (SEEG) contact classification cross-validation (randomly split 20% vs. 80% test vs. train set over 1000 iterations) when using different feature sets. AUC, mean area under the receiver-operating-characteristic curve; Crit.P., criticality properties; Sync.D., synchrony derivatives; * indicates differences (repeated *t*-test, $-\log_{10}[p]$ in sequence: 62.1, 39.9, 117.8, Benjamini–Hochberg false discovery rate [FDR] corrected). Dashed lines indicate surrogate (Surro) mean ($n_{surro} = 1000$). (D) Mean AUC ($n = 55$) of within-patient SZ classification; * and ** indicate differences (unpaired *t*-test, $-\log_{10}[p] = 2.2$ and 6.1, respectively (Benjamini–Hochberg FDR corrected). Error bars indicate SD; dashed lines indicate surrogate mean ($n_{surro} = 1000$). (E) All-to-all SEEG contact similarity matrix. Boxes demarcate three clusters. Cluster 1 likely represented the epileptogenic network. (F) Probability distribution of SZ likelihood (L_{SZ}) for each cluster defined in panel E. (G and H) L_{SZ} of SZ and non-SZ (nSZ) of (G) cluster 1 and (H) clusters 0 and 2. (I–L) Intracluster group average of (I) local efficiency (LE), (J) BiS index, (K) fE/I index, and (L) detrend fluctuation analysis (DFA). For intercluster differences in features see Figure S8. Cc, clustering coefficient; Cort, cortical; EVC, eigenvector centrality; Norm', normalized; Sig.Neg.Corr., significant negative correlation; Sig.Pos.Corr. significant positive correlation; We, effective weight.

preceding supercriticality. The average absolute correlation between criticality features was .2 ± .17 (±SD), with a maximum reaching .8. The synchrony features showed only positive correlations across bands, with an average of .46 ± .24 and a maximum reaching .9 (Figure S6J). The correlation between the criticality and synchrony features was weak, with an average of .05 ± .04 and a maximum reaching .22 (Figure 4B), implying that they represent nonredundant physiological processes. Because both feature families showed differentiating effects for SZ, combining them would likely offer better classification accuracy than using any individual features alone.

As a precaution, we took two additional procedures to validate that criticality and synchrony constituted useful features for SZ classification (Supplementary Methods). First, we assessed feature importance for cohort-level SZ classification with the Shapley Additive Explanations values. This revealed that $\gamma_{1\text{-}2}$ band BiS and fE/I, β band BiS, and $\delta-\theta$ band LE were among the most important features (Figure S7A). Next, we conducted a population level cross-validation with 1000 independent iterations, each of which was a random 80:20% partition (training set: test set) of the contacts. We tested SZ classification using criticality alone, synchrony alone, and combining criticality and synchrony and for only cortical contacts and all contacts with subcortical included. Combining all features ("All" in Figure 4C) yielded the highest accuracy, with an average area under the receiver operating characteristic curve (AUC) reaching .85 ± .002 (±SD). This offered proof-of-concept for within-patient SZ classification.

Lastly, within-patient SZ classification was conducted with leave-one-out validation, that is, a patient's contacts served as the test set and the remaining subjects as the training set. Using all features again yielded the best accuracy, with an AUC of .73 ± .16 for all contacts and .72 ± .16 for cortical contacts (Figure 4D). There was no difference in AUC when using cortical only and all contacts (repeated t-test, $p > .55$). Synchrony features were more potent than criticality features for population-level classification (Figure 4C), whereas criticality features were more potent for within-patient SZ classification (Figure 4D).

3.5 | Unsupervised classification reveals EpiNet-like cluster

Our last question concerned whether the pathological brain network extended beyond the SZ into areas clinically identified as healthy nSZ. A positive finding would constitute evidence to support the EpiNet hypothesis. We evaluated the similarity between contact features and then subjected the resulting similarity matrix to cluster analysis (Supplementary Materials). Across a range of partition solutions from two to nine clusters, three principal clusters remained stable in their constituent contacts and representative of the cohort. Therefore, we chose the three-cluster partition for analyses (Figure 4E).

We investigated whether any clusters represented distinct pathophysiological profiles by jointly analyzing them with supervised SZ classification and physician-identified SZ. The supervised classifier assigned each contact an SZ likelihood (L_{SZ}) ranging from 0 to 100%, indicating how likely it was an SZ based on models learned from the training set. Physicians assigned each contact a binary label, indicating whether it was an SZ or nSZ. The contacts in cluster 1 (pink, Figure 4F) were assigned larger L_{SZ} than those in clusters 0 and 2 (unpaired t-test $-\log_{10}(p) > 10^{15}$ and >234.2, respectively), whereas contacts in clusters 0 and 2 had no differences (unpaired t-test, $-\log_{10}(p) < .35$). The probability of observing a physician-identified SZ in cluster 1 (48.8%) was more than twice as large as that in clusters 0 and 2 (23.0% and 21.2%, respectively), further supporting that cluster 1 represents pathophysiology, indicative of the EpiNet (Figure 4G,H).

The contacts in cluster 1 exhibited elevated local efficiency (Figure 4I) and eigenvector centrality (Figure S8) in δ to γ_1 band, larger bistability and I-dominance in β and $\gamma_{1,2}$ band (Figure 4J,K), and higher DFA in $\gamma_{1,2}$ band (Figure 4L). The concurrent large first- and second-order connectivity suggests that cluster 1 contacts act as central nodes while showing aberrant criticality as predicted by our computational model.

4 | DISCUSSION

With our putative mechanistic EZ biomarkers, we extracted neuronal features from interictal SEEG and trained supervised classifiers to localize the SZ against gold standard clinical SEEG localization. We showed with computational modeling that a high seizure risk dynamical regime was characterized by high degree of bistability, I-dominance, and aberrant LRTCs in local synchrony. The SEEG analyses revealed that, even during interictal resting state when the EpiNet is thought to be inactive, SZ samples exhibited features closely matching the model in the high seizure risk regime. Meanwhile, these SZ samples exhibited strong interareal synchrony, implying a large-scale tendency toward supercriticality. Supervised classifiers trained on all features yielded more accurate SZ classification (AUC = .85) than using any individual feature alone (AUC = .6–.7). Unsupervised classification identified three principal clusters, one of which, cluster 1, exhibited high seizure risk features. Interestingly, 50% of the cluster 1 samples were healthy nSZ identified by physicians during electroclinical

assessment (see Section 2.2). Colocalization using supervised and unsupervised classification revealed that 25% of these nSZ samples in cluster 1 were considered to be SZ by the supervised classifier, suggesting that the EpiNet may extend beyond the areas clinically identified as SZ.

4.1 | Strong positive feedback leads to high bistability, I-dominance, and elevated seizure risk

In our model, I-dominance was seen exclusively inside a critical regime with high bistability, where the model demonstrated a lowered coupling threshold to exhibit hypersynchrony. In the interictal SEEG, both the SZ contacts and the contacts from the pathological cluster were characterized by concurrent I-dominance and strong bistability in the β–γ bands. Positive feedback has been suggested to be a universal mechanism leading to bistability near criticality.[35] In our model, the positive feedback was an abstract state-dependent term. In more realistic models such as the Wilson–Cowan model, several synaptic mechanisms such as strong firing-rate-dependent excitation and inhibition—and a combination of both—may lead to bistability in neuronal activity.[29] Strong inhibition could be both the cause and consequence of epileptic seizures due to a pathological depolarizing γ-aminobutyric acid substrate.[41] Other studies also have suggested that the positive feedback may be facilitated through cellular and molecular level mechanisms such as increased dendritic excitability,[42] metabolic anomalies,[43] or neuroinflammation.[44] Nonetheless, theoretical research has suggested an association between positive feedback and high resource demand,[36] which makes neurons susceptible to pathology.[45]

4.2 | EZ is hypothetical core of EpiNet

The concept of the EZ has evolved over several decades,[15,17,39,46] but the clinical objective of EZ localization—long-term seizure freedom—has remained unchanged.[47] The EZ represents the EpiNet that generates seizures, and, hypothetically, multiple surgical solutions could be considered with corresponding clinical constraints weighted.[12]

An individual EZ might consist of components such as lesion zone, seizure zone, and irritative zone,[39] some of which may overlap. This could account for why individual biomarkers often localize EZ inconsistently across subjects.[7,8] The low postsurgical seizure freedom in many patients has suggested that pathological networks were not fully mapped with existing biomarkers/approaches. We found that combining all criticality and synchrony biomarkers yielded the highest classification accuracy compared to using any single biomarkers alone. This finding indicated that combining criticality and synchrony provided synergistic information, supporting the multicomponent hypothesis for EZ.[39]

4.3 | EpiNet represents pathological network more extended than previously thought

The EpiNet-like cluster entailed both nSZ and clinically identified SZ. As spatiotemporal organization of seizure can be highly variable across patients,[48,49] it is possible that these nSZ contacts did not show any seizure activity, or they might occasionally show seizure activity that was not captured during the electroclinical assessments. However, unsupervised classifiers trained on features extracted from only 10 min of interictal SEEG revealed that these nSZs and the SZs shared similar feature profiles. This implied that the entirety of the EZ could encompass brain areas extending outside conventionally defined SZ. Alternatively, although not explicitly involved in seizure activity like the SZ, these nSZs could be linked to the altered structural connectivity within the EpiNet, potentially suggesting regions of future seizure network spread or kindling.

In contrast, some SZs were assigned to the two remaining clusters that did not show clear signs of pathophysiology. We postulated these atypical SZs might be peripheral nodes in the EZ. Due to the unavailability of the structural connectome data, we could not simulate large-scale synchrony to test this idea. Future efforts should be directed toward elucidating the dissociation revealed here.

4.4 | Integrating brain criticality and synchrony: Mechanistic EZ biomarkers

Physicians identified the SZ using peri-ictal and ictal SEEG and other relevant assessments.[4] We extracted criticality and synchrony features from interictal SEEG, ensuring no seizures 1 h before and after these data. We used the SZ labels to train classifiers to identify the SZ based on these features, and classification accuracies were variable with an AUC of $.73 \pm .16$. This indicated that, in some subjects, a significant number of SZ and nSZ contacts were not clearly separated in the feature domain, potentially due to complexity in individual EZ dynamics. Spatial organization of SZ may show considerable variability over time.[48] Seizure or epileptiform activities typically occur at specific phases in seizure cycles across temporal scales, ranging from ultradian or circadian, to weekly or monthly

and even yearly (seasonal) cycles.[49] The spatiotemporal complexity could be further compounded by ambiguity of the SZ due to variances in seizure electrophysiological signatures[4] and an absence of clear clinical definitions for some seizure types.[50] Additionally, collapsing narrowband features may result in loss of useful information regarding the SZ (Supplementary Materials 1.5.4).

Taking these factors into consideration, we recognize that one snapshot of 10-min interictal SEEG may not adequately capture the EZ dynamics in every patient, which likely contributed to the variability in classification accuracy. Applying our approach in a time-resolved manner to assess EZ spatiotemporal dynamics would yield valuable insights into individual EZs across different phases of the seizure cycles, particularly in complex cases of DRE.

5 | CONCLUSIONS

Combining criticality and synchrony assessments with data science approaches will promote data sharing and open a new avenue for novel clinical applications such as advanced surgical planning and prediction or real-time monitoring of epileptogenicity.

AUTHOR CONTRIBUTIONS

Conceptualization: Sheng H. Wang and J. Matias Palva. *Funding acquisition:* J. Matias Palva, Satu Palva, and Sheng H. Wang. *Methodology:* Sheng H. Wang. *Software:* Sheng H. Wang, Vladislav Myrov, and Gabriele Arnulfo. *Formal analysis:* Sheng H. Wang. *Resources:* Gabriele Arnulfo and Lino Nobili. *Data curation:* Gabriele Arnulfo and Vladislav Myrov. *Visualization:* Sheng H. Wang, Philippe Ciuciu, and J. Matias Palva. *Original draft:* Sheng H. Wang and J. Matias Palva. *Writing:* Sheng H. Wang, Paul Ferrar, Lino Nobili, Philippe Ciuciu, Satu Palva, and J. Matias Palva. *Supervision:* J. Matias Palva.

ACKNOWLEDGMENTS

This project was funded by Academy of Finland grants (SA 253130 and 296304) awarded to J.M.P.; a Sigrid Jusélius Foundation grant awarded to S.P. and J.M.P.; NEXTGENERATIONEU (NGEU), the Ministry of University and Research, and National Recovery and Resilience Plan project MNESYS (PE0000006; A Multiscale Integrated Approach to the Study of the Nervous System in Health and Disease; DN. 1553 11.10.2022) awarded to L.N. and G.A. The theoretical work was partially funded the Ella and Georg Ehrnrooth Foundation (S.H.W., 14-10553-2). Analytical tool development, data analyses, and publication preparation were supported by the Finnish Cultural Foundation postdoc fellowship (00220071) and the Sigrid Jusélius Foundation fellowship (210527), awarded to S.H.W. S.H.W. is also supported by the DARLING project (Projet-ANR-19-CE48-0002) awarded to P.C. We are grateful for the support.

CONFLICT OF INTEREST STATEMENT

None of the authors has any conflict of interest to disclose.

DATA AVAILABILITY STATEMENT

Compliance with Italian governing laws and ethical committee regulations prohibits the sharing of raw data and patient details. However, interim data and final results that support the findings of this study can be obtained from the corresponding authors upon reasonable request.

ETHICS STATEMENT

This study was approved by the ethical committee (ID 939) of Niguarda Hospital, Milan, Italy, and was performed according to the Declaration of Helsinki. We confirm that we have read the Journal's position on issues involved in ethical publication and affirm that this report is consistent with those guidelines.

PATIENT CONSENT STATEMENT

Before electrode implantation, all patients gave written informed consent for participation in research studies and for publication of the results. The patient SEEG data and clinical information were handled anonymously.

ORCID

Sheng H. Wang https://orcid.org/0000-0002-6226-6213
Gabriele Arnulfo https://orcid.org/0000-0002-1140-0320
Lino Nobili https://orcid.org/0000-0001-9317-5405

REFERENCES

1. Fisher RS, Cross JH, French JA, Higurashi N, Hirsch E, Jansen FE, et al. Operational classification of seizure types by the international league against epilepsy: position paper of the ILAE Commission for Classification and Terminology. Epilepsia. 2017;58:522–30.
2. Devinsky O, Vezzani A, O'Brien TJ, Jette N, Scheffer IE, De Curtis M, et al. Epilepsy. Nat Rev Dis Prim. 2018;4:1–24.
3. Fisher RS, Van Emde BW, Blume W, Elger C, Genton P, Lee P, et al. Response: definitions proposed by the international league against epilepsy (ILAE) and the International Bureau for Epilepsy (IBE) [4]. Epilepsia. 2005;46:1426–41.
4. Di Giacomo R, Uribe-San-Martin R, Mai R, Francione S, Nobili L, Sartori I, et al. Stereo-EEG ictal/interictal patterns and underlying pathologies. Seizure. 2019;72:54–60.
5. Cardinale F, Rizzi M, Vignati E, Cossu M, Castana L, d'Orio P, et al. Stereo-electroencephalography: retrospective analysis of 742 procedures in a single centre. Brain. 2019;142:2688–704.
6. Bulacio JC, Bena J, Suwanpakdee P, Nair D, Gupta A, Alexopoulos A, et al. Determinants of seizure outcome after resective surgery following stereoelectroencephalography. J Neurosurg. 2022;136:1638–46.

7. Perucca P, Gotman J. Delineating the epileptogenic zone: spikes versus oscillations. Lancet Neurol. 2022;21:949–51.
8. Bernabei JM, Li A, Revell YA, Smith RJ, Gunnarsdottir KM, Ong IZ, et al. Quantitative approaches to guide epilepsy surgery from intracranial EEG. Brain. 2023;146:2248–58.
9. Zweiphenning W, van MA, C Klink NE, S Leijten FS, Ferrier CH, Gebbink T, et al. Intraoperative electrocorticography using high-frequency oscillations or spikes to tailor epilepsy surgery in the Netherlands (the HFO trial): a randomised, single-blind, adaptive non-inferiority trial. Lancet Neurol. 2022;21:982-93.
10. Cossu M, Fuschillo D, Casaceli G, Pelliccia V, Castana L, Mai R, et al. Stereoelectroencephalography-guided radiofrequency thermocoagulation in the epileptogenic zone: a retrospective study on 89 cases. J Neurosurg. 2015;123:1358–67.
11. van Lanen RHGJ, Colon AJ, Wiggins CJ, Hoeberigs MC, Hoogland G, Roebroeck A, et al. Ultra-high field magnetic resonance imaging in human epilepsy: a systematic review. NeuroImage Clin. 2021;30:102602.
12. Miller KJ, Fine AL. Decision-making in stereotactic epilepsy surgery. Epilepsia. 2022;63:2782–801.
13. Matarrese MAG, Loppini A, Fabbri L, Tamilia E, Perry MS, Madsen JR, et al. Spike propagation mapping reveals effective connectivity and predicts surgical outcome in epilepsy. Brain. 2023;146:3898–912.
14. Gnatkovsky V, De Curtis M, Pastori C, Cardinale F, Lo Russo G, Mai R, et al. Biomarkers of epileptogenic zone defined by quantified stereo-EEG analysis. Epilepsia. 2014;55:296–305.
15. Bartolomei F, Guye M, Wendling F. Abnormal binding and disruption in large scale networks involved in human partial seizures. EPJ Nonlinear Biomed Phys. 2013;1:1–16.
16. Khambhati AN, Davis KA, Oommen BS, Chen SH, Lucas TH, Litt B, et al. Dynamic network drivers of seizure generation, propagation and termination in human neocortical epilepsy. PLoS Comput Biol. 2015;11:1–19.
17. Proix T, Bartolomei F, Guye M, Jirsa VK. Individual brain structure and modelling predict seizure propagation. Brain. 2017;140:641–54.
18. Wang HE, Woodman M, Triebkorn P, Lemarechal JD, Jha J, Dollomaja B, et al. Delineating epileptogenic networks using brain imaging data and personalized modeling in drug-resistant epilepsy. Sci Transl Med. 2023;15:1–15.
19. Jirsa V, Wang H, Triebkorn P, Hashemi M, Jha J, Gonzalez-Martinez J, et al. Personalised virtual brain models in epilepsy. Lancet Neurol. 2023;22:443–54.
20. Buzsáki G, Schomburg EW. What does gamma coherence tell us about inter-regional neural communication? Nat Neurosci. 2015;18:484–9.
21. Gunnarsdottir KM, Li A, Smith RJ, Kang JY, Korzeniewska A, Crone NE, et al. Source-sink connectivity: a novel interictal EEG marker for seizure localization. Brain. 2022;145:3901–15.
22. Fuscà M, Siebenhühner F, Wang SH, Myrov V, Arnulfo G, Nobili L, et al. Brain criticality predicts individual synchronization levels in humans. Nat Commun. 2023;14:4736.
23. Beggs JM. The criticality hypothesis: how local cortical networks might optimize information processing. Philos trans R soc a math Phys. Eng Sci. 2008;366:329–43.
24. Linkenkaer-Hansen K, Nikouline VV, Palva JM, Ilmoniemi RJ. Long-range temporal correlations and scaling behavior in human brain oscillations. J Neurosci. 2001;21:1370–7.
25. Beggs JM, Plenz D. Neuronal avalanches in neocortical circuits. J Neurosci. 2003;23:11167–77.
26. Bruining H, Hardstone R, Juarez-Martinez EL, Sprengers J, Avramiea AE, Simpraga S, et al. Measurement of excitation-inhibition ratio in autism spectrum disorder using critical brain dynamics. Sci Rep. 2020;10:9195.
27. Zimmern V. Why brain criticality is clinically relevant: a scoping review. Front Neural Circuits. 2020;14:1–34.
28. Meisel C, Schulze-Bonhage A, Freestone D, Cook MJ, Achermann P, Plenz D. Intrinsic excitability measures track antiepileptic drug action and uncover increasing/decreasing excitability over the wake/sleep cycle. Proc Natl Acad Sci. 2015;112:14694–99.
29. Wilson HR, Cowan JD. Excitatory and inhibitory interactions in localized populations of model neurons. Biophys J. 1972;12:1–24.
30. Freyer F, Roberts JA, Ritter P, Breakspear M. A canonical model of multistability and scale-invariance in biological systems. PLoS Comput Biol. 2012;8:e1002634.
31. Wang SH, Siebenhühner F, Arnulfo G, Myrov V, Nobili L, Breakspear M, et al. Critical-like brain dynamics in a continuum from second-to first-order phase transition. J Neurosci. 2023;43(45):7642–56.
32. Steriade M, Nunez A, Amzica F. A novel slow (<1 Hz) oscillation of neocortical neurons in vivo: depolarizing and hyperpolarizing components. J Neurosci. 1993;13:3252–65.
33. Holcman D, Tsodyks M. The emergence of up and down states in cortical networks. PLoS Comput Biol. 2005;2:e23.
34. Freyer F, Aquino K, Robinson PA, Ritter P, Breakspear M. Bistability and non-gaussian fluctuations in spontaneous cortical activity. J Neurosci. 2009;29:8512–24.
35. Buendía V, di Santo S, Bonachela JA, Muñoz MA. Feedback mechanisms for self-organization to the edge of a phase transition. Front Phys Ther. 2020;8:1–17.
36. di Santo S, Villegas P, Burioni R, Muñoz MA. Landau–Ginzburg theory of cortex dynamics: scale-free avalanches emerge at the edge of synchronization. Proc Natl Acad Sci. 2018;115:E1356–E1365.
37. Thom R. Structural stability and morphogenesis. 1st ed. Boca Raton: CRC Press; 1972.
38. Villa Martín P, Bonachela JA, Levin SA, Muñoz MA. Eluding catastrophic shifts. Proc Natl Acad Sci. 2015;112:E1828–E1836.
39. Zijlmans M, Zweiphenning W, van Klink N. Changing concepts in presurgical assessment for epilepsy surgery. Nat Rev Neurol. 2019;15:594–606.
40. Arnulfo G, Wang SH, Myrov V, Toselli B, Hirvonen J, Fato MM, et al. Long-range phase synchronization of high-frequency oscillations in human cortex. Nat Commun. 2020;11:5363.
41. van van Hugte EJH, Schubert D, Nadif Kasri N. Excitatory/inhibitory balance in epilepsies and neurodevelopmental disorders: depolarizing γ-aminobutyric acid as a common mechanism. Epilepsia. 2023;64:1975–90.
42. Dimakopoulos V, Gotman J, Stacey W, Von Ellenrieder N, Jacobs J, Papadelis C, et al. Protocol for multicentre comparison of interictal high-frequency oscillations as a predictor of seizure freedom. Brain Commun. 2022;4:1–8.
43. Rho JM, Boison D. The metabolic basis of epilepsy. Nat Rev Neurol. 2022;18:333–47.
44. Vezzani A, French J, Bartfai T, Baram TZ. The role of inflammation in epilepsy. Nat Rev Neurol. 2011;7:31–40.

45. Bullmore E, Sporns O. The economy of brain network organization. Nat Rev Neurosci. 2012;13:336–49.
46. Li A, Huynh C, Fitzgerald Z, Cajigas I, Brusko D, Jagid J, et al. Neural fragility as an EEG marker of the seizure onset zone. Nat Neurosci. 2021;24:1465–74.
47. Luders H, Engel J, Munari C. Update on surgical treatment of the epilepsies. Surgical treatment of the epilepsies. New York: Raven Press; 1993.
48. Schroeder GM, Diehl B, Chowdhury FA, Duncan JS, de Tisi J, Trevelyan AJ, et al. Seizure pathways change on circadian and slower timescales in individual patients with focal epilepsy. Proc Natl Acad Sci USA. 2020;117:11048–58.
49. Karoly PJ, Rao VR, Gregg NM, Worrell GA, Bernard C, Cook MJ, et al. Cycles in epilepsy. Nat Rev Neurol. 2021;17:267–84.
50. Fisher RS, Scharfman HE, DeCurtis M. How can we identify ictal and interictal abnormal activity? Adv Exp Med Biol. 2014;813:3–23.

SUPPORTING INFORMATION

Additional supporting information can be found online in the Supporting Information section at the end of this article.

How to cite this article: Wang SH, Arnulfo G, Nobili L, Myrov V, Ferrari P, Ciuciu P, et al. Neuronal synchrony and critical bistability: Mechanistic biomarkers for localizing the epileptogenic network. Epilepsia. 2024;65:2041–2053. https://doi.org/10.1111/epi.17996